International Journal of Hydrogen Energy 202 (2026) 153072

Contents lists available at ScienceDirect

International Journal of Hydrogen Energy

journal homepage: www.elsevier.com/locate/he

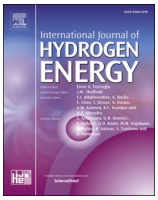

Catalytically active plate heat exchanger for flexible hydrogen release from perhydro benzyltoluene

P. Nathrath [a], T. Hein [a], M. Li [b], F. Lederle [b], P. Wasserscheid [a,c,d], E.G. Hübner [b,e], P. Schühle [a,*]

[a] Friedrich-Alexander-Universität Erlangen-Nürnberg, Institute of Chemical Reaction Engineering, Egerlandstr. 3, Erlangen, DE-91058, Germany
[b] Fraunhofer Heinrich Hertz Institute, HHI, Fiber Optical Sensor Systems, Am Stollen 19 H, Goslar, DE-38640, Germany
[c] Forschungszentrum Jülich GmbH, Helmholtz Institute Erlangen-Nürnberg for Renewable Energy (IEK-11), Cauerstr. 1, Erlangen, DE-91058, Germany
[d] Forschungszentrum Jülich GmbH, Institute for Sustainable Hydrogen Economy (INW), Wilhelm-Johnen-Straße, Jülich, DE-52428, Germany
[e] Clausthal University of Technology, Institute of Organic Chemistry, Leibnizstr. 6, Clausthal-Zellerfeld, DE-38678, Germany

ARTICLE INFO

Keywords:
LOHC
Dehydrogenation
Catalytic plate reactor
Benzyltoluene
Dynamic operation

ABSTRACT

In the future energy system, hydrogen is expected to play an important role as a large-scale energy storage option. The liquid organic hydrogen carrier (LOHC) technology enables safe and long-term hydrogen storage using the existing tank infrastructure available from the current fossil fuel products. On-demand hydrogen release from LOHC systems followed by its use in fuel cells or combined cycle power plants (CCP) can provide green electricity to the grid in a load flexible manner. However, to serve fast load changes in the grid, highly dynamic LOHC dehydrogenation reactors with fast response times are required. In this study, we demonstrate a catalytic plate reactor (CPR) derived from the design of conventional plate heat exchangers for the continuous and dynamic dehydrogenation of perhydro benzyltoluene. The surface of corrugated heat exchanger plates in the size of 15 × 15 cm has been catalytically activated by spray-coating and laser texturing techniques. These activated plates have been investigated in continuous operation under different stationary reaction conditions (290–340 °C; 2.5–5 bar_a and 1–3 $g_{H12\text{-}BT}$ min^{-1}) achieving technical relevant degrees of dehydrogenation (DoDHs) above 80 %, activities up to 0.27 mg_{H2} cm^{-2} min^{-1} and stable hydrogen release for several hundred hours of operation. Furthermore, the new CPR exhibited short hysteresis times when feed flow or reaction temperature were dynamically changed demonstrating impressively its suitability for on-demand hydrogen provision. Finally, the CPR was successfully operated following the dynamic load profile of a technical relevant CCP scenario.

1. Introduction

The share of renewable energies in the electricity mix is increasing worldwide [1,2]. In Europe, renewables, mainly photovoltaics and wind power, now account for 38 % of the electricity production and it is projected to reach over 70 % by 2030 [3]. While this shift is essential for the targeted defossilization, it introduces new challenges to power grid stability and market dynamics [4]. The generation of renewable energy is volatile due to daily sunlight cycles, seasonal wind patterns, and changing weather conditions. When these renewable technologies make up a larger share of electricity production, the need for load flexible technologies grows to quickly balance electricity demands [5–7]. In today's energy grid, fast-reacting combined cycle power (CCP) plants provide this flexible backup power by natural gas combustion. But these power plants emit several million tons of CO_2 every year [8,9]. In addition, methane emissions to the atmosphere during natural gas production and transport contribute significantly to climate change. Therefore, fossil-free and climate friendly alternative solutions for flexible and on-demand electricity production are of high interest.

Hydrogen technologies can offer attractive options in this context [10–14]. Water electrolysis converts renewable electricity into green hydrogen in times and at locations of abundant green electricity [15,16]. Fuel cells or CCP plants retrofitted for the use of green hydrogen can re-electrify hydrogen to compensate mismatches between power supply and demand [16–19]. In-between hydrogen has to be stored or even transported safely and with high energy density. Liquid organic

* Corresponding author.
E-mail address: Patrick.Schuehle@fau.de (P. Schühle).

https://doi.org/10.1016/j.ijhydene.2025.153072
Received 12 October 2025; Received in revised form 26 November 2025; Accepted 15 December 2025
Available online 19 December 2025

hydrogen carrier (LOHC) systems are an excellent option for this purpose, as they can store hydrogen as a liquid at ambient temperature and pressure using existing fuel infrastructure [20,21]. LOHC systems are based on reversibly binding hydrogen to organic carrier molecules. Catalytic hydrogenation of the LOHC species results in hydrogen-loaded carrier molecules. The hydrogen can be released on demand via catalytic dehydrogenation and the so-obtained hydrogen-lean LOHC compound can be used for another storage cycle [20,22].

The pair benzyltoluene (H0-BT)/perhydro benzyltoluene (H12-BT) is a particularly promising LOHC system [23], that is characterized by a high storage capacity of 6.2 wt%, good thermal stability, a liquid state over a wide temperature range and the availability in technical quantities at a moderate price [23,24]. The dehydrogenation of H12-BT (see Scheme 1) is operated in presence of a heterogeneous catalyst, typically platinum on a porous alumina support [25–27] and at low pressures between 1 and 5 bar [16]. Due to the endothermic character (63.5 ± 1.05 kJ mol_{H2}^{-1} [28]) of the reaction, temperatures beyond 260 °C are usually applied for thermodynamic reasons. The main side product of the reaction is methylfluorene (MF) which is formed consecutively through dehydrocyclization of the aromatic H0-BT species (see Scheme 1) [29]. However, doping the platinum catalyst system with a certain amount of strongly Pt-bound sulfur reduces this path of side product formation [30].

The continuous dehydrogenation of H12-BT has mostly been studied in fixed-bed reactors [21,31–34], although efficient heat supply to the catalyst has been found a major challenge. The limited heat transfer by the point-to-point contact of spherical catalyst pellets in combination with the strongly endothermal dehydrogenation reaction and feed evaporation typically results in a radial temperature profile in the reactor tube with significantly lower temperatures in the center of the catalyst bed compared to the reactor wall [35]. This inhomogeneous temperature profile limits the space-time yield in fixed-bed LOHC dehydrogenation reactors and complicates its dynamic operation [36].

To address the goal of load-flexible power production using carrier-released hydrogen the dynamic operation of dehydrogenation reactors is necessary. In contrast to fixed-bed reactors, catalytic plate reactors (CPR) can achieve efficient heat provision to the reaction system facilitating dynamic operation [21,36,37]. The CPR concept consists of metal plates, which are coated with a heterogeneous catalyst layer and are directly heated from the backside. This design fundamentally enhances heat transfer compared to conventional fixed-bed reactors by leveraging large-area metallic heat conduction rather than relying on limited point contacts between particles and heat transfer via fluid convection. Consequently, the formation of significant temperature gradients across the catalytically active area of the CPR can be avoided, even in highly endothermic or exothermic reactions under dynamic load changes [36–38]. By using corrugated metal plates, e.g. with a chevron pattern, more turbulent flow regimes can be realized, further enhancing the heat and mass transfer capabilities of the CPR [38,39]. Moreover, the CPR is characterized by a compact and modular design, enabling a flexible scale-up to the desired power output [36,40]. Notably, the small dimensions and adaptable scalability of the CPR are not only favorable for large-scale applications but also for mobile and decentral units.

The performance of the CPR module is greatly affected by the nature of the catalyst layer and its preparation [41]. Typically, a porous alumina support is generated by coating a metallic plate (e. g. a heat exchanger plate) with a sol-gel composite dispersion consisting of γ-Al_2O_3 and boehmite. Various coating techniques can be used to obtain the desired porous support layer on the plate [42,43]. Spray-coating is well-established, fast, and scalable process for the preparation of support layers on open sight geometries [44,45]. The active metal can then be introduced by wet impregnation. For this purpose, the support layer is impregnated with a solution containing the platinum precursor. Subsequent reduction in hydrogen atmosphere forms the catalytically active surface, e.g. for the dehydrogenation of H12-BT [36,46].

An interesting alternative to spray coating is ultrashort-pulse laser texturing. This technique is based on the modification of a metallic plate surface by laser pulses with a usual duration of pico- to femtoseconds [47,48]. The precise ablation of surface material leads to three-dimensional micro- and nanostructures on the plate surface [49]. Additionally, performing laser texturing in ambient air or oxygen results in the formation of porous metal oxide structures. These laser induced nano foam (LINF) structures provide high surface areas and have a thickness of up to several hundred micrometers [50–53]. In our previous work, we could demonstrate the successful application of LINF to produce aluminum oxide coatings that served as catalysts supports in small-scale LOHC dehydrogenation applications [54].

In this publication, we report on the continuous operation of a CPR for the dynamic hydrogen release from H12-BT under technically relevant conditions (>290 °C, >2.5 bar_a). The CPR under investigation contains two opposite plates (plate size 15 × 15 cm) with a total catalytically active area of 426.4 cm^2. Our study compares two techniques, spray-coating and laser texturing, to produce the aluminum oxide support layer on the corrugated metal plates. The spray-coated and wet-impregnated plates are intensively tested in H12-BT dehydrogenation in long-term operation. As a major aim of our study is to test the CPR in dynamic operation, its response time to flexible load changes is determined. Finally, we apply the relative flexible load changes of a technical CCP plant to our CPR in order to evaluate whether the CPR technology can provide hydrogen on demand for such a real-life dynamic application.

2. Methods

2.1. Preparation of spray-coated catalyst plates

First, primer layers of the alumina support were applied on the sandblasted and cleaned stainless steel plates (15 × 15 cm, material 1.4404, Kelvion PHE GmbH). The preparation of the primer dispersion was carried out by mixing 1.44 g of the boehmite component Dispersal® (Sasol Germany), 43.89 g of deionized water, and 1.79 g of nitric acid (69 %, VWR Chemicals). After dispersing 2.88 g of the aluminum oxide powder Catalox® (Sasol Germany) into the mixture, the sol was aged for 4 h with stirring at 1000 rpm. Two layers of the primer dispersion were manually spray-coated onto the corrugated stainless steel plates. The solvent was removed with unheated air flow, followed by drying in an oven at 60 °C over night.

Afterwards, a sol-gel composite dispersion for the alumina support

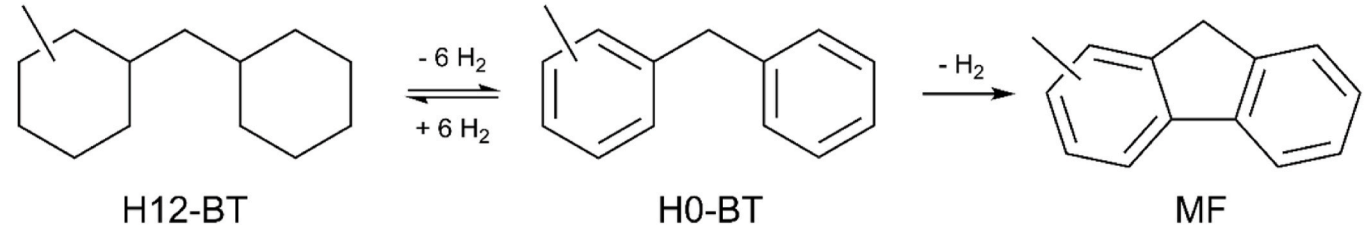

Scheme 1. Dehydrogenation reaction of perhydro benzyltoluene (H12-BT) to benzyltoluene (H0-BT) and consecutive formation of the by-product methylfluorene (MF) by deep dehydrogenation.

layer was prepared following the procedure reported in our previous publication [46]. An automated spray-coating system, consisting of an automatic sprayer connected to a motorized linear guiding system, was used to produce homogeneous coatings. The metal plate, combined with an octahedral template, was placed centric in the spray-coating setup and heated constantly to 80 °C from the backside. During spray-coating, the sprayer followed linear and horizontal trajectories at a constant velocity of 250 mm s^{-1}. The procedure was repeated until the desired amount of dispersion was applied, with approximately 4 min of drying time between each spray-coating cycle. The coated plates were calcined at 550 °C in air for 6 h, using a heating ramp of 2 K min^{-1}. Platinum was applied via wet impregnation using a 14.8 wt% aqueous platinum sulfite acid solution (Strem) in 600 mL of deionized water. After 16 h of impregnation, the catalyst plates were dried and then reduced at 440 °C in a 5 % H_2 in N_2 atmosphere for 4 h. ICP-AES (Ciros CCD, SPECTRO Analytical Instruments GmbH) was used to analyze the actual Pt loading on the catalyst plates by measuring the remaining platinum content in the precursor solution.

2.2. Preparation of laser-structured catalyst plates

Non-planar aluminum plates (square shaped approx. 150 x 150 × 6 mm, 1 mm plate thickness, AlMg3 EN AW-5754) with an embossed flow profile were pretreated with an ytterbium pulsed fiber laser (YLPN-1-1x350-100, IPG Laser GmbH & Co. KG, Burbach, Germany). The detailed procedure can be found in the ESI E.1. Afterwards, femtosecond laser structuring was applied. The general setup for this procedure has been published previously [55–57]. The settings of the AMPHOS 400 Yb:YAG high power laser system are coherent with those of our previous publication [54]. Due to the rather long focus depth of 8 mm of the beam, a height correction for laser processing the chevron shaped flow profile was not necessary (see Figure ESI 2 (a)). The focus point was set to the middle of the height profile. Using single beam operation, these laser settings would result in a surface processing rate of 16.8 min cm^{-2}. To speed up the process, a diffractive optical element (DOE) was applied (sep. angle 1.37°, DS-238-J-Y-A, HOLO/OR) to split the primary laser beam, reducing the processing rate to 8.4 min cm^{-2}. All experiments were conducted in a stainless steel processing chamber under ambient conditions (20 °C, relative humidity RH = 40 %) with ablation products being removed from a constant air flow of 12 m s^{-1}. The plates were clamped seamlessly onto a matching chevron shaped steel base to ensure sufficient cooling (see Figure ESI 1). All samples were cleaned by ultrasonication in deionized water and isopropanol for 0.5 min each. After cleaning, the samples were dried in a stream of nitrogen and stored under ambient conditions.

The active metal platinum is introduced onto the laser induced nano foam (LINF) structure via a two-step wet impregnation process with platinum sulfite acid solution. The subsequent reduction was identical to the procedure of the spray-coated catalyst plates. The Pt loading on the laser-structured plates was determined by ICP-AES analysis of a small fraction of the catalyst layer.

2.3. Characterization of the plate catalysts

The number and strength of acidic sites on the support material of the plate catalyst was investigated by temperature programmed desorption of ammonia (NH_3-TPD) in a Thermo Scientific TPDRO 1100. For the measurement, 300 mg of the sample is pretreated at 440 °C in He, cooled to 100 °C and exposed to a stream of 10 % NH_3/He until saturation. Excess NH_3 is flushed with He before the samples are cooled to 30 °C. The sample is heated to 850 °C in 10 K min^{-1} steps under He and the thermal conductivity of the offgas is monitored.

High-angle annular dark field scanning transmission electron microscopy (HAADF-STEM) is utilized (TalosF200i, Thermo Fisher Scientific) to evaluate the platinum nanoparticle distribution. Projected areas of at least 500 visible particles per sample were analyzed and converted to a circle equivalent diameter to calculate the volume-area-mean particle size d_{VA} (eq. (1)) [58].

$$d_{VA} = \frac{\sum n_i d_i^3}{\sum n_i d_i^2} \tag{1}$$

Thermo-gravimetric analysis with mass spectrometry coupling (TGA-MS) was used to determine the proportion of coke precursors and carbon deposits on the catalyst after H12-BT dehydrogenation. Reversibly adsorbed organic components were removed prior to analysis in a soxhlet setup with cyclohexane (reflux conditions for min. 2 h, afterwards drying over night at 60 °C). The measurements were carried out with a TA Instruments SDT 2960 coupled with a Pfeiffer Vacuum Thermostar (GSD 300 T1) mass spectrometer. TGA measurements were conducted by heating the sample to 800 °C (5 K min^{-1}) in synthetic air and the weight of the sample as well as the gas phase composition was continuously monitored.

X-ray diffraction (XRD) patterns of the samples have been recorded on a PANalytical X'Pert Pro MPD (Philips) equipped with a Cu Kα radiation source and are displayed in the ESI.

2.4. Stationary dehydrogenation experiments

A CAD cross section view of the CPR used in this work is shown in Fig. 1 (a). Two catalyst plates with a combined macroscopic catalytic area of 426.4 cm^2 were installed in the CPR. Table 1 summarizes the properties, respective support mass, platinum mass, and loading of the tested plate sets.

One plate is fixed in the bottom part of the CPR as illustrated in Fig. 1 (b) and the second plate on top with both catalytically activated sides facing each other. The two parts of the CPR are sealed with a graphite gasket and heated by four heating cartridges each. Additional pictures of the CPR in opened and closed state can be found in the ESI (Figure ESI 3). During all experiments the CPR was fixed in a vertical position, resulting in an up-flow reaction configuration. The reaction temperature was monitored and controlled by a thermocouple in each reactor part just below the milled negative of the plates.

The applied dehydrogenation unit (simplified flow scheme and photograph shown in the ESI, see Figure ESI 4) was inertized with argon and heated to the target reaction temperatures (290–340 °C) under continuous hydrogen flow. After setting the reaction pressure to 2.5–5 bar_a using a pressure regulator (Equilibar), the plant was flooded with perhydro benzyltoluene (H12-BT, degree of hydrogenation >99 %). Subsequently, the feed flow was set to 1 $g_{H12\text{-}BT}$ min^{-1} or 3 $g_{H12\text{-}BT}$ min^{-1} by adjusting the feedstock pump. As soon as a steady feed flow was established, continuous H12-BT dehydrogenation was performed in the CPR for 25 h. The product hydrogen was separated from the liquid, cooled in a condenser and purified by an active carbon filter to remove traces of LOHC vapor. The hydrogen flow was determined by a mass-flow meter (MFM) (Bronkhorst, El-Flow Prestige). The productivity P was calculated by Equation (2), considering the mean hydrogen flow $\dot{V}_{H_2}$ over 20 h time on stream, the density of hydrogen at standard conditions ρ_{STP,H_2}, and the total platinum mass m_{Pt}. The catalytic activity A, based on the macroscopic catalytic area S_{cat}, was derived from Equation. (3). Furthermore, the power density ϕ of the CPR can be calculated from the lower heating value (LHV) of the released H_2 and the reaction volume V_R (see Equation (4)).

$$P = \frac{\dot{V}_{H_2} \cdot \rho_{STP,H_2}}{m_{Pt}} \tag{2}$$

$$A = \frac{\dot{V}_{H_2} \cdot \rho_{STP,H_2}}{S_{cat}} \tag{3}$$

$$\phi = \frac{\dot{V}_{H_2} \cdot \rho_{STP,H_2} \cdot LHV_{H_2}}{V_R} \tag{4}$$

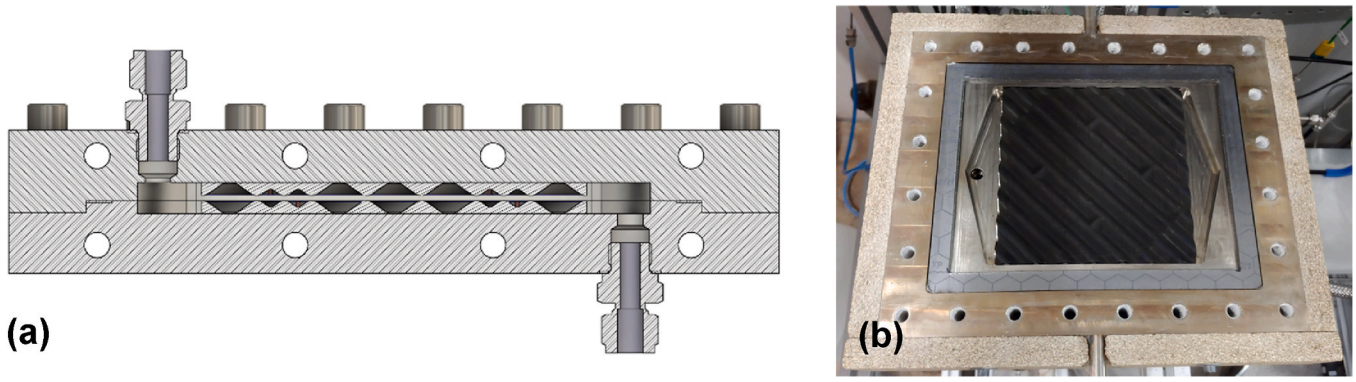

Fig. 1. CAD cross section view of the employed CPR (a) and close-up photo of the opened CPR (b).

Table 1
Properties of the tested plate sets (SC – spray-coated, LT – laser-textured), their platinum mass and loading measured via ICP-OES.

Plate set	Support mass	Platinum mass	Platinum loading
Spray-coated (SC)	13.54 g	0.498 g	1.17 mg cm^{-2}
Laser-textured (LT)	–	0.512 g	1.20 mg cm^{-2}

Liquid samples were taken after the first hour and then in 3-h intervals afterwards. The last three liquid samples were used to determine the average degree of dehydrogenation (DoDH) by refractometry (Krüss DR6300-T). The DoDH, which represents the ratio of hydrogen actually released from a given LOHC material related to its maximum releasable hydrogen, was calculated from the refractive index with the correlation reported by M. Geiβelbrecht [59]. Additionally, the DoDH and methylfluorene (MF) content of the last sample were measured by GC-FID (Shimadzu, GC-2010 Plus).

2.5. Dynamic dehydrogenation experiments

For the dehydrogenation studies with spray-coated plates in dynamic operation, the reactor temperatures and feed flows were adjusted at different levels between 310 and 320 °C and 1–3 $g_{H12\text{-}BT}$ min^{-1} and a fixed pressure of 4 bar_a. To assess the response time of the hydrogen output, the reaction was first started with a fixed heating ramp of 2.6 K min^{-1} till 310 °C. After reaching a stable operation, the temperature was rapidly increased to 320 °C. Then, the temperature was decreased back to the starting level of 310 °C. The feed flow was kept constant at 1 $g_{H12\text{-}BT}$ min^{-1} over the whole period. In a second experiment, the procedure was carried out with the feed flow starting at 1 $g_{H12\text{-}BT}$ min^{-1}, then elevated to 3 $g_{H12\text{-}BT}$ min^{-1}, and subsequently decreased back to the starting level at a fixed temperature of 310 °C. In a third experiment, both parameter adjustments were carried out simultaneously (starting level: 310 °C, 1 $g_{H12\text{-}BT}$ min^{-1}; raised level: 320 °C, 3 $g_{H12\text{-}BT}$ min^{-1}). Between each of the three experiments, the reactor was cooled to room temperature and the catalysts were dried to maintain equal starting conditions. The stability of the catalysts and the hydrogen release under dynamic conditions were evaluated by feed flow, and heating ramp variations.

2.6. Dynamic tests following a realistic application scenario

The load profile of a CCP plant has been chosen as comparative system to demonstrate the feasibility of our CPR under dynamic operation conditions. CCP plants (typically burning natural gas) represent the state-of-the-art power generation method to cover peak loads of electricity in Germany. The tested load profile was derived from a dataset of the CCP plant "München Süd GuD2 DT 60" from July 18, 2023, published by Fraunhofer Institute for Solar Energy Systems (ISE) (see Figure ESI 11) [60]. To ensure continuous monitoring of the laboratory plant, the dataset was simplified and shortened to a 5 h load profile. Furthermore, we applied a maximum heating ramp of 5.3 K min^{-1} reflecting the technical capabilities of our experimental setup.

3. Results

3.1. Fabrication of heat exchanger plates with catalytically active surfaces

For the successful implementation of the CPR technology, high mechanical stability and catalytic activity of the catalyst-coated heat exchanger plates are required. Therefore, our first set of experiments aimed at the proper selection of a suitable fabrication technique for the Pt–S/Al_2O_3 coatings on the plates. For this purpose, we compared plates fabricated by spray coating and by laser texturing in the dehydrogenation of H12-BT at three different sets of operation parameters and a feed flow of 1 $g_{H12\text{-}BT}$ min^{-1}. Please note, that several analytical data on similar plates produced via the two fabrication methods can be found in our previous publications [46,54]. With 0.498 g (SC) and 0.512 g (LT), both plate catalyst systems possess an equivalent amount of platinum on the same macroscopic plate area (see Table 1). The results follow a similar qualitative trend for both systems. In terms of DoDH and activity (see Fig. 2 (a) and 2 (b)) notable differences in the achieved values for the two plate catalyst systems can be observed. The degrees of dehydrogenation under equilibrium conditions ($DoDH_{eq}$, black horizontal lines in Fig. 2 (a)) have been calculated according to Rüde et al. [29].

Under reference conditions (300 °C, 2.5 bar_a and 1 $g_{H12\text{-}BT}$ min^{-1}), the LT plates achieved a DoDH of 39.9 %, while the SC plates reached 56.9 %. Consequently, as illustrated in Fig. 2 (b), the activity is approximately 25 % higher for the SC plates compared to the LT plates. With reaction conditions that allow the DoDHs to approach equilibrium ($DoDH_{eq}$), the differences between the two types of plate fabrications decrease, as expected. The maximum DoDHs are observed for both plate reactors at 340 °C, 5 bar_a, and a feed rate of 1 $g_{H12\text{-}BT}$ min^{-1}. Here, the LT plates reach a DoDH of 83.8 %, which is only a bit lower than the 86.6 % achieved with the SC plates. Based on the LHV of H_2 and the reaction volume of the CPR (105 mL (LT) and 107 mL (SC), respectively), these activities translate into power densities of 1.07 MW m^{-3} (SC) and 1.01 MW m^{-3} (LT), respectively.

In general, the results shown in Fig. 2 suggest slower reaction kinetics for the laser-textured system compared to the spray-coated system. One potential reason for this discrepancy may be in the different pore structures obtained with the different fabrication techniques. As shown in our previous work, the LT support material exhibits a surface area of approximately 30 m^2 g^{-1} and mainly small mesopores in the range of 3–4 nm diameter [54]. The spray-coated plates, in contrast, have a substantially higher surface area of approximately 150 m^2 g^{-1} and wider mesopores with diameters of 11–12 nm [46]. The wider pores

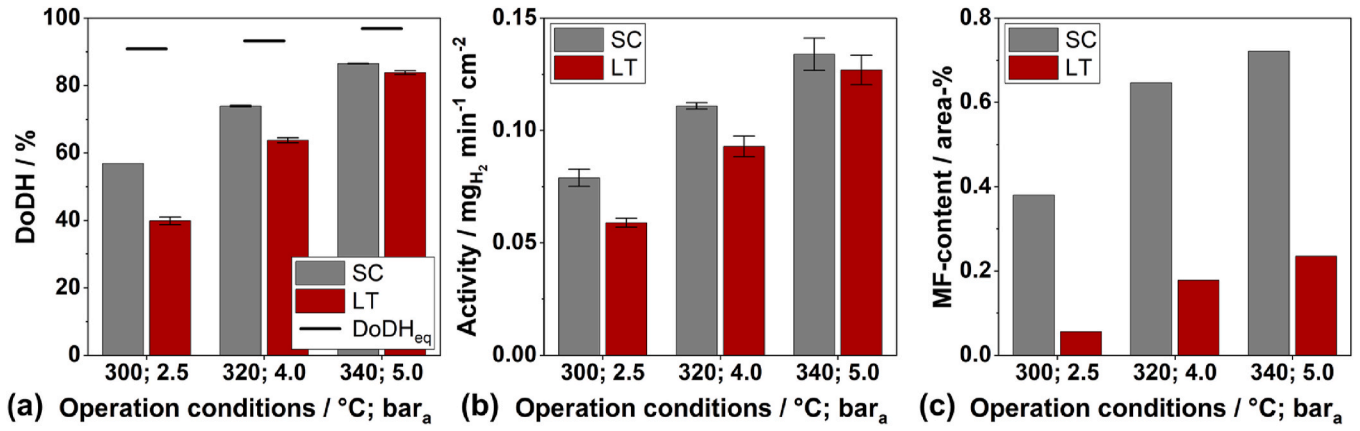

Fig. 2. Comparison of the DoDH (a) activity (b) and MF-content (c) achieved with laser-textured (LT) and spray-coated (SC) plate catalysts for selected operation parameters and a feed flow rate of 1 $g_{H12\text{-}BT}$ min^{-1}.

in the spray-coated plate catalysts improve the diffusional transfer of H12-BT to the active sites, bubble nucleation, and bubble oscillation, as suggested by previous studies [61,62]. In addition, the lower internal surface of the LT-plate coatings results in larger Pt particles during the wet impregnation process (lower Pt dispersion), as known from literature [63,64]. This is confirmed by our HAADF-TEM images (shown in Fig. 3) that reveal a significantly increased average Pt particle size in the case of the laser-textured catalyst plates. While a mean Pt particle diameter d_{VA} of 2.73 nm was found on the LT-plate, the d_{VA} on the SC plates was only 1.95 nm. The larger platinum particles in the case of the

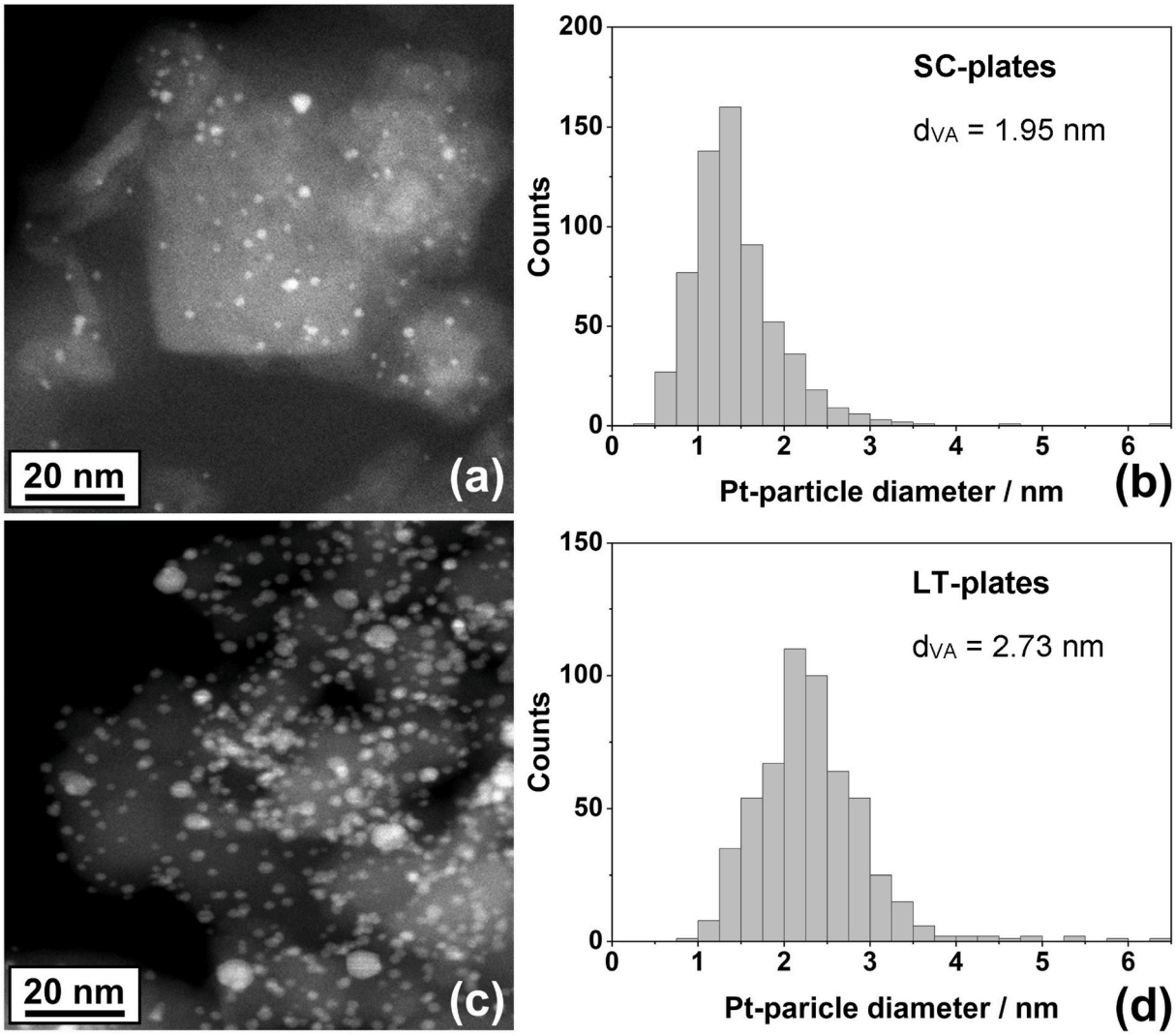

Fig. 3. HAADF-TEM image and Pt particle size distribution of the spray-coated (SC) catalyst plate (a)/(b) and laser-textured (LT) plate catalyst (c)/(d).

LT plates result in a lower active metal surface compared to the SC plates at even overall platinum mass on both coatings.

Interestingly, the dehydrogenation reaction promoted by the LT plates forms significantly less MF even at similar DoDH levels (see Fig. 2 (c)). For example, at 340 °C, 5 bar_a and 1 $g_{H12\text{-}BT}$ min^{-1}, the SC-plates produced 0.72 % MF at a DoDH of 86.6 %, while the MF content with the LT-plates was only one third (0.24 %) at a very similar DoDH of 83.8 %. One possible explanation for this behavior is the higher share of Pt particles with diameters above 2 nm in the LT plate catalyst. Such bigger particles exhibit a lower proportion of low-coordinated platinum sites (edge or corner atoms of the particle), which are known to strongly adsorb aromatic products and thus facilitate oxidative cyclization reactions [30,65]. However, as the majority of such centers are selectively blocked by the sulfur doping of the catalyst, this alone might not explain the remarkably lower MF formation of the LT-plates.

Another factor influencing the formation of by-products, such as MF, can be the surface acidity of the support material [30,66,67]. Although both systems predominantly contain γ-alumina (see Figure ESI 12), the smaller surface area of the LT plate leads to a considerably lower concentration of acidic surface centers, as demonstrated by the NH_3-TPD measurements shown in Fig. 4.

By mathematical integration of the NH_3 desorbing from the catalyst material, the amount of acidic centers can be calculated. As a result, 375.7 μmol g^{-1} acidic centers were found for the LT support material, while the amount of acidic sites was three times higher in the case of the spray-coated material (1008.9 μmol g^{-1}). The combination of a smaller number of acidic sites along with the reduction of the share of corner and edge atoms due to the larger platinum particle size explains, therefore, the remarkably lower MF-formation of the laser-textured plate catalysts. The higher acidity of the SC support furthermore results in more and stronger anchoring points for the Pt precursor contributing to the better Pt dispersion on the SC catalyst.

For all further studies, the SC plate catalysts have been selected due to their superior dehydrogenation activity and the excellent scalability of the fabrication process. While laser texturing excels with high precision and control over surface patterns, scaling of the technology is currently limited by long processing times per plate (approx. 28 h). Nevertheless, it remains noteworthy that the use of LT plates represents a novel approach in catalysis, which was applied in this work for the first time on this scale (213.2 cm^{-2} per plate) and with such high platinum loadings (approx. 1.20 mg cm^{-2}).

3.2. Detailed parameter variation with spray-coated plates

In the following, the dehydrogenation of H12-BT is studied in our CPR module using SC catalytic plates under steady-state conditions. Our goal was to explore how reaction temperature and reactant flows influence the observed hydrogen release rate, DoDH and MF formation. The experiments were performed at 4 bar_a, to operate above the vapor pressure of H12-BT even at highest adjusted temperature. The results are shown in Fig. 5 (a)–(d).

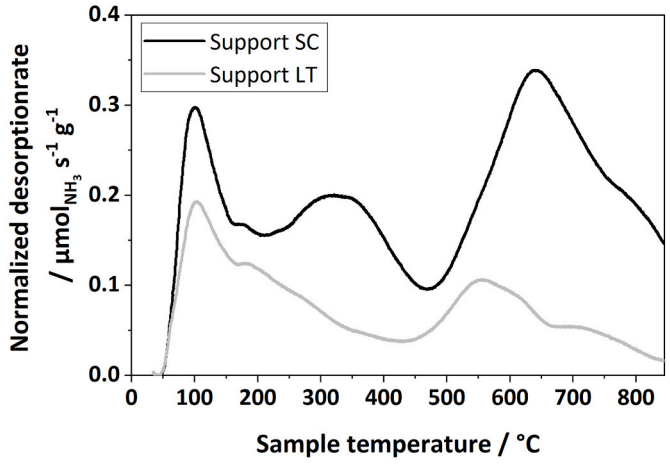

Fig. 4. NH_3-TPD experiments of the spray-coated (SC) and the laser-textured (LT) coatings.

With an increase of the reaction temperature from 290 to 340 °C, the DoDH increases from 32.5 to 91.3 % at a flow rate of 1 $g_{H12\text{-}BT}$ min^{-1} and from 26.9 to 64.2 % at 3 $g_{H12\text{-}BT}$ min^{-1} (see Fig. 5 (a)). The increase in H12-BT feed flow reduces the liquid residence time. As a result, the activity and productivity of the plate catalysts increases at the expense of lower DoDHs (compare Fig. 5(c) and (d)). In fact, the triple feed rate approximately doubles the activity and productivity achieved with the SC plates. The maximum hydrogen release is achieved at 340 °C and 3 $g_{H12\text{-}BT}$ min^{-1} reaching activities of 0.27 mg_{H2} min^{-1} cm^{-2}. This translates into a power density of the CPR of 2.16 MW m^{-3}. In case of the dehydrogenation parameters leading to the highest DoDH of 91.3 % (340 °C and 1 $g_{H12\text{-}BT}$ min^{-1}) the power density is still as high as 1.11 MW m^{-3}.

The high dehydrogenation activity at 340 °C causes a greatly reduced LOHC vapor pressure in the reactor and, consequently, serious LOHC evaporation under these conditions. To counteract this effect, the reaction pressure was increased to 5 bar_a for the operation at 340 °C in the following experiments. A comparison of the dehydrogenation results at 340 °C and the two pressure levels can be found in the supporting information (Figure ESI 6). According to Le Chatelier's principle, the increase in total pressure reduces the equilibrium conversion of the dehydrogenation reaction. However, at 5 bar_a only a minor effect on DoDH and activity is found. We conclude that the negative effect of the pressure increase on the reaction equilibrium (and thus the driving force of the reaction) is at least partially compensated by a reduction of H12-BT evaporation. This results in a higher share of LOHC in the liquid phase in the reactor which is linked to better heat transfer and a longer residence time of the LOHC-molecules in the reactor.

In Fig. 5 (b), the amount of MF side product formation is shown for each operation point. Operation points at higher temperatures show higher DoDHs and also higher MF formation. This can be explained by the fact that MF forms in a consecutive reaction from H0-BT. Interestingly, there is a clear influence of H12-BT flow rate on the MF formation even at the same DoDH levels (see Fig. 6).

A similar behavior of MF formation was observed by Ellert et al. using a finned-tube reactor with Pt–S/Al_2O_3 catalyst [68]. We hypothesize that the higher liquid flow and the higher liquid content leads to more turbulence in the reactor. This increases mass and heat transfer and reduces the contact time of the H0-BT product within the catalyst coating preventing consecutive reactions. Improved catalyst wetting may also play a role. It has been found in previous studies that wetting problems can occur in particular with vertical reactor orientations and high gas loads as present in the H12-BT dehydrogenation [69]. We expect that the corrugation angle of the plates could serve as an important parameter to optimize catalyst wetting in the CPR under high gas load conditions.

3.3. Stability in long-term dehydrogenation experiments

To evaluate operational long-term stability of our SC catalyst plates, we first plotted a particular reference operation point that was frequently adjusted in our parameter variation studies (as shown in Figs. 2 and 5, Figure ESI 5 and Figure ESI 6) over time-on-stream (TOS). Multiple adjustment of this reference operation point (300 °C, 2.5 bar_a and 1 $g_{H12\text{-}BT}$ min^{-1}) served during our parameter studies to check whether the catalyst is undergoing deactivation over the course of the study. The results are shown in Fig. 7.

Noteworthily, the dehydrogenation performance remained stable for more than 530 h TOS which included several reactor start-up and cool-down events. In the last reference experiment, between 805 and 825 h

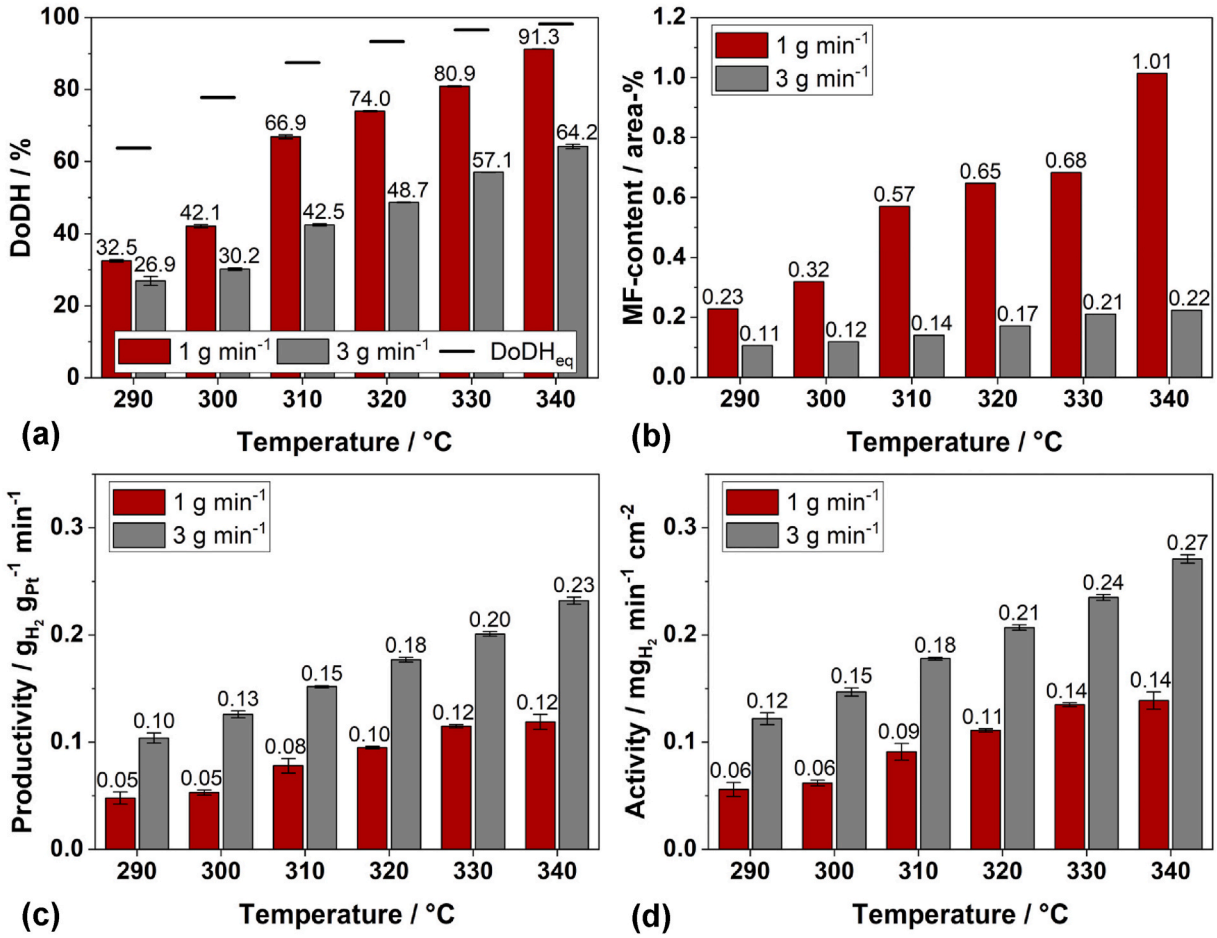

Fig. 5. Achieved DoDH (a), formed MF-content (b), productivities (c), and activities (d) for the temperature and H12-BT flow variation at 4 bar_a using spray-coated plates (SC) in the CPR.

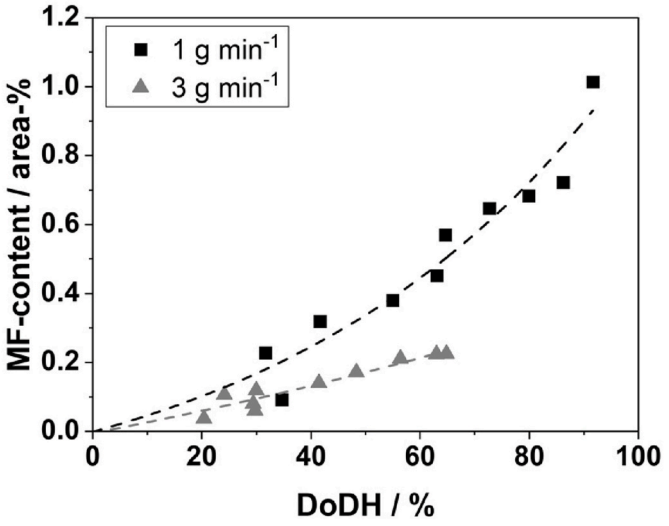

Fig. 6. MF formation with spray-coated plates (SC) in the CPR over achieved DoDH values at different feed flow rates.

TOS, the DoDH values of the product LOHC were approximately 11 % lower. We account this to the experiments under harsh conditions (at 340 °C and 4 or 5 bar_a) between 530 h and 800 h TOS and hypothesize that the slightly lower dehydrogenation performance is a result of coke formation on the catalyst. Especially at high temperatures and high gas phase hold-ups in the reactor, coke precursors that would normally be washed away by fresh LOHC-material, can remain on the catalyst surface and this can lead to the formation of carbonaceous deposits [30,70,71]. To evaluate the presence of carbonaceous deposits on the catalyst surface further, TGA-MS measurements were conducted (see Figure ESI 7). In comparison to a fresh catalyst the used SC-plate showed noteworthy weight loss and CO_2 formation in the temperature range 200–500 °C supporting the presence of carbonaceous deposits after long-term reaction.

Furthermore, the used SC plates were visually examined after the dehydrogenation experiments. In Fig. 8 a comparison of an SC plate before and after the continuous dehydrogenation experiments is shown. Overall, no significant defects or delamination of the coating, apart from minor indentations at the contact points of overlaying plates, were found. These indentations originate from the direct contact of the two plates caused by the compression of the graphite sealing due to the mounting pressure of the reactor parts.

To complement our catalyst stability studies, also the catalytic LT plates were subjected to a simplified stability test in a stationary long-term dehydrogenation experiment at 330 °C, 4 bar_a and 1 $g_{H12\text{-}BT}$ min^{-1} (for results, see Figure ESI 8). Despite the relatively harsh conditions, no significant deactivation was found within the operation time of 120 h. Therefore, the LT plates can also be considered as stable catalyst systems under the here applied reaction conditions.

3.4. *Dynamic dehydrogenation for flexible H_2-supply*

Apart from stationary hydrogen release, the dynamic operation of a

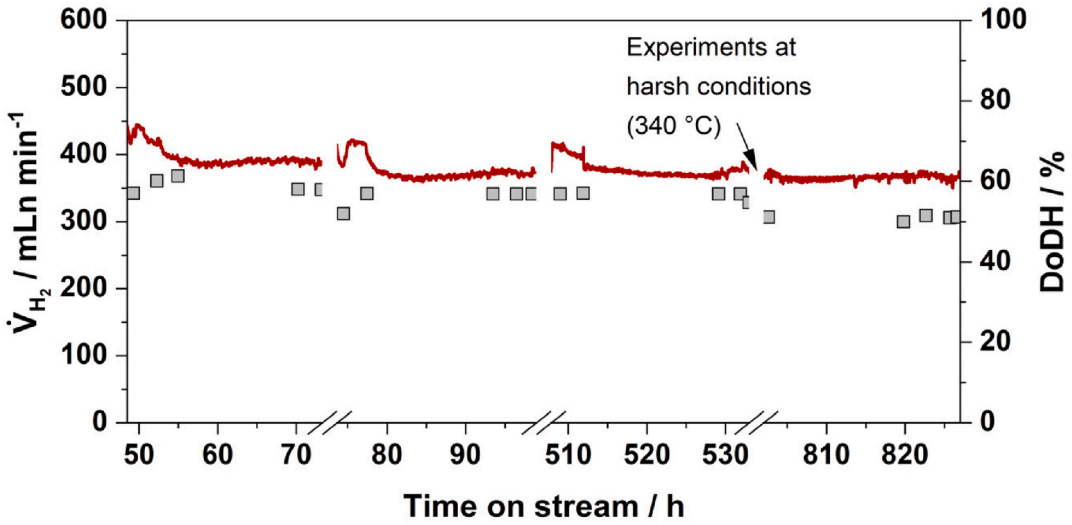

Fig. 7. Long-term dehydrogenation stability of the spray-coated plate catalysts over the total time on stream at reference conditions (300 °C, 2.5 bar_a, 1 $g_{H12\text{-}BT}$ min^{-1}).

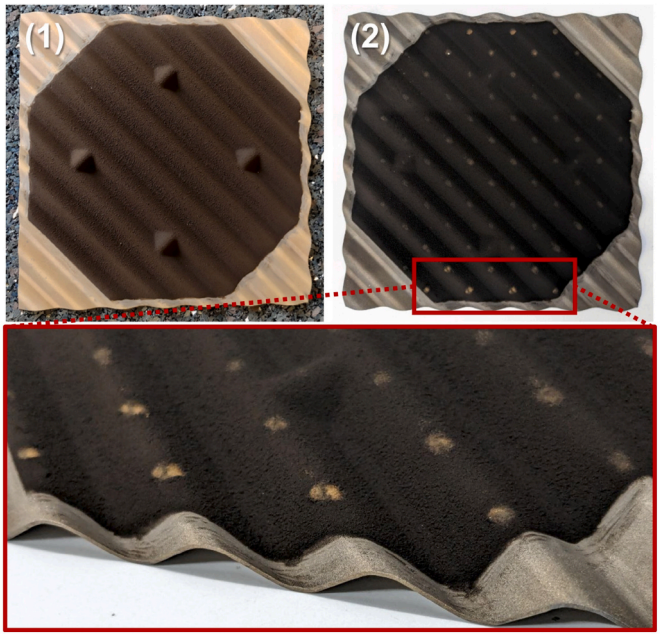

Fig. 8. Spray-coated plates before (1) and after (2) application in continuous H12-BT dehydrogenation experiments.

LOHC dehydrogenation reactor is of particular relevance to accomplish a demand oriented supply of H_2 for subsequent re-electrification. Fig. 9 shows the response in H_2 release for our SC plate setup after temperature increase (I), after an increase of the H12-BT flow (II), and after a simultaneous adjustment of both parameters (III). Between each of these dynamic response experiments, the CPR was transferred into a standby state (ambient temperature, pressure approx. 2 bar_a) and restarted again, using an identical start-up protocol. This protocol includes step-wise heating of the reactor with a rate of 2.6 K min^{-1} to the reaction temperature of 310 °C. The reaction temperature was reached within about 2 h. The product H_2 volume stream was around 440 mLn min^{-1} under the applied reference conditions (310 °C; 1 $g_{H12\text{-}BT}$ min^{-1}).

In the temperature variation period (see I) in Fig. 9), an increase in temperature led to an immediate short overshoot of the H_2 flow rate to a maximum of 615 mLn min^{-1}. During the following 30 min the system levelled down to a stable release of 540 mLn min^{-1} which represents a 20 % increase in hydrogen production compared to the reaction at 310 °C. The DoDH at 320 °C increased to 70 % compared to 57 % DoDH at 310 °C. After 1.5 h at this stable operation point (overall experimental time of 4.8 h in the graph), the temperature was reduced again to 310 °C and the system came back to its initial productivity at this conditions within 17 min TOS. The observed fast response to lower hydrogen productivity reflects the endothermic nature of the reaction.

In the flow variation period (see II) in Fig. 9), the H12-BT flow was increased from 1 to 3 $g_{H12\text{-}BT}$ min^{-1}. This led to an increase of the hydrogen release rate to a stable value of 760 mLn min^{-1} within 10 min. Because the higher H12-BT flow leads to a reduced residence time of H12-BT in the reactor, the DoDH dropped from initial 57 % (1 $g_{H12\text{-}BT}$ min^{-1}) to approx. 39 % (3 $g_{H12\text{-}BT}$ min^{-1}) within this variation. Finally, both parameter changes were executed in combination (variation period III) in Fig. 9). In this case, the H_2 release increased to approximately 900 mLn min^{-1} (with a DoDH of 48 %). The entire variation experiment showed that our CPR can be operated quite flexibly despite its high thermal inertia and relatively low catalyst mass. In the ESI (see Figure ESI 10), we show another long-term experiment with flow and temperature variations that further confirms the excellent stability of our SC plate equipped CPR over a total of 26 h TOS.

3.5. *Mimicking the load change of a combined cycle power plant*

In the future, hydrogen released from LOHC might be used for load-flexible power generation to buffer the volatility of renewable energy sources. Fig. 10 illustrates such a scenario, in which the main electricity supply is covered by renewables. In times of overproduction, H_2 is produced and stored in LOHC. In times of low wind and sun, the stored H_2 can be released in a CPR and subsequently re-electrified.

With the following experiments, we want to show that our new CPR reactor can cope with the dynamic load change requirements of such an application case. As benchmark for the load profile we have chosen the CCP plant „München Süd GuD2 60“ [60]. The selected data points and shortened profile are shown in the ESI (see Figure ESI 11). The output power was normalized to allow a comparison with our laboratory scale investigations (see Figure ESI 11 (b)). The modular design of the CPR facilitates up-scaling of the hydrogen output by simple up-numbering of the parallel plate slits. Assuming uniform behavior across all plate slits, the dynamics observed in the single-slit CPR can be used as indication for the dynamics of the stack of plate reactors. Fig. 11 shows the normalized power output of the CPR at 320 °C, 4 bar_a and varying feed flow to achieve the required H_2 release dynamics, as well as the

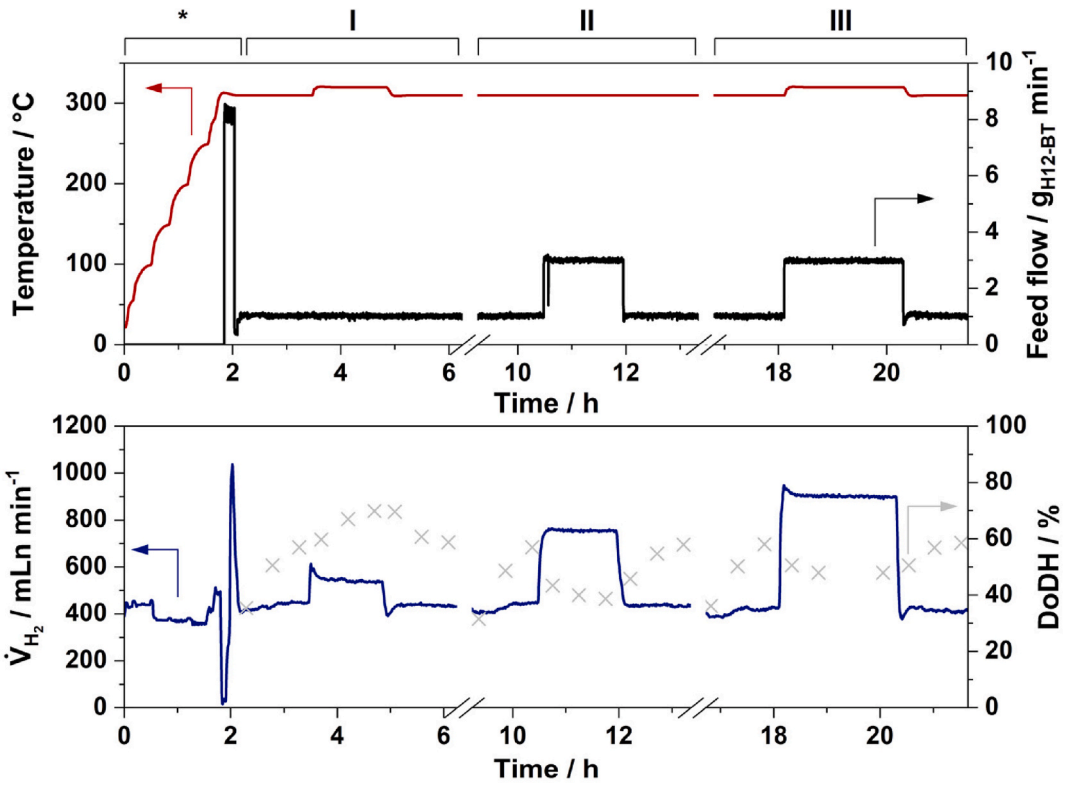

Fig. 9. Response of the CPR under dynamic conditions including changes in temperature (310–320 °C, phase I), feed flow (1–3 g_{H12-BT} min^{-1}, phase II), and simultaneous changes of both parameters (phase III) (pressure 4 bar_a; phase * represents the reactor start-up from ambient conditions).

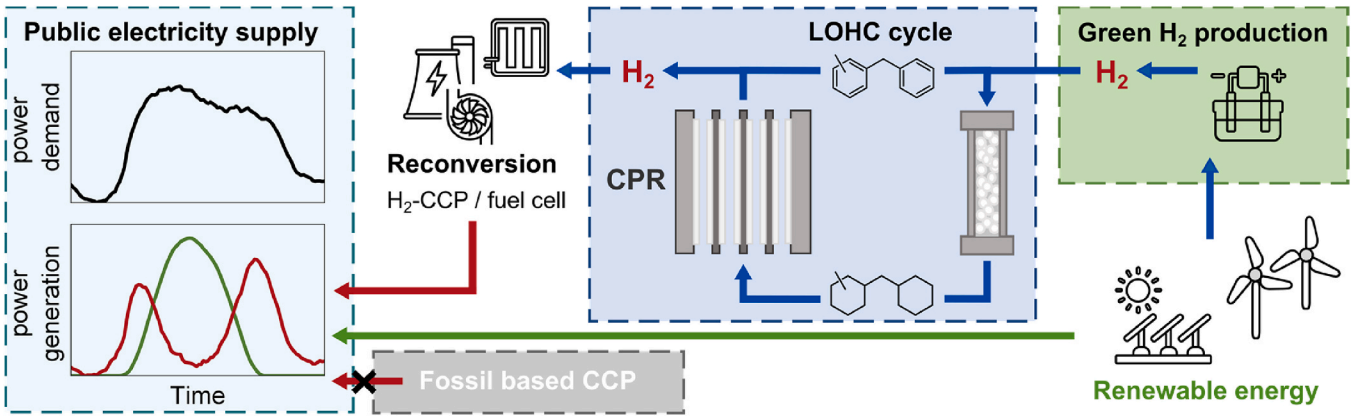

Fig. 10. Schematic of a possible integration of the hydrogen release from LOHC in a CPR to buffer the volatility of renewable energy production.

simplified load profile of the CCP.

The maximum heating rate in our experimental setup was 5.3 K min^{-1}. With this value, the start-up time in our device could be shortened to approximately 70 min. 60 min of this time can be accounted to the heating to reach the reaction temperature and another 10 min to flood the reactor with H12-BT. The CCP plant, in contrast, starts within 15 min from a standby-state of the plant. From a time-on-stream of 1.5 h we found good conformity of the normalized power output of our CPR and the technical data for the CCP plant (the deviation between 3.8 h and 4.5 h TOS was introduced purposedly to the CPR to check the unit's behavior on lower load levels). To catch-up with the CCP plant load profile again, a short time of 7 min proved sufficient. Subsequently, the subtle load changes of the technical CCP plant could be very well followed in our CPR unit as depicted in the enlarged section on the right side of Fig. 11. To validate the shut-down rate of the CPR, a 10 min delay was added holding the last operation point at the end of the experiment. Still, the CPR managed a faster decrease in power output compared to the CCP plant profile. The better power decrease rate can be attributed to the endothermic dehydrogenation in combination with the good heat conductivity of the metal plates. Therefore, the catalyst temperature can be reduced very quickly below the temperature level at which the dehydrogenation stops for thermodynamic and kinetic reasons.

In general, we can deduct from this experiment, that the CPR can follow technical relevant load changes of a real-life CCP plant. Thus, hydrogen release from H12-BT using our CPR-concept proves sufficiently dynamic to serve an on-demand power provision scenario with a CCP unit as re-electrification technology.

4. Conclusion

In this study, we tested a novel CPR with spray-coated and laser-textured catalytic plates for the load-flexible provision of hydrogen

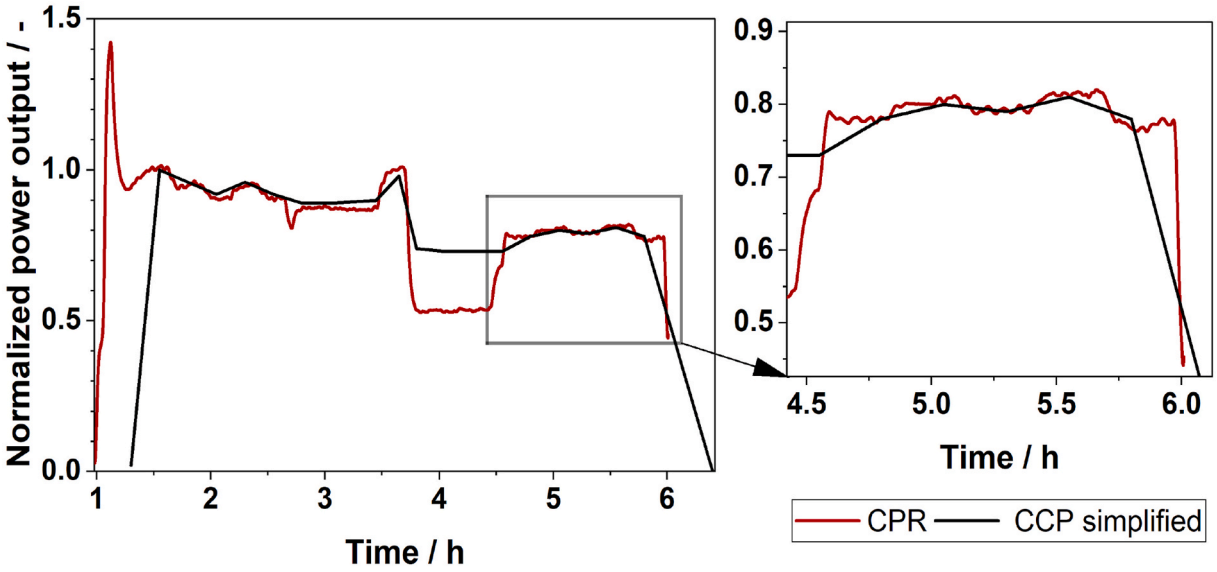

Fig. 11. Normalized power output of the CPR (320 °C, 4 bar_a, heat up phase without feed flow approximately 1 h, varying feed flow 0.8–3.1 $g_{H12\text{-}BT}$ min^{-1}) and a simplified load profile of a CCP plant.

from the LOHC system H0-BT/H12-BT. We demonstrate that high DoDH above 80 % can be effectively achieved using such CPR systems with catalyst coated corrugated plates. Under comparable conditions of 340 °C, 5 bar_a and 1 $g_{H12\text{-}BT}$ min^{-1}, the laser-textured catalyst plates reached a DoDH of 83.8 %, while 86.6 % was achieved using the spray-coated plates. By increasing the feed flow rate to 3 $g_{H12\text{-}BT}$ min^{-1}, a peak activity 0.27 mg_{H2} min^{-1} cm^{-2} could be realized with the spray-coated plates. We attribute the superior catalytic activity of the spray-coated plates to a better platinum dispersion in the porous support layer of the catalyst. Interestingly, the larger Pt-nanoparticles obtained on the laser-textured samples resulted in a reduced MF side product formation at comparable DoDHs.

The long-term stability of our CPR module was verified in H12-BT dehydrogenation experiments over several hundred hours operation time. No significant decrease in hydrogen production rate was observed over an extended test period of 530 h (including varying operation conditions) when the reaction temperature was kept at 330 °C or lower. At 340 °C reaction temperature, however, a slow catalyst deactivation was found, which can be attributed to the formation of carbonaceous deposits under these conditions where total evaporation of the LOHC material and catalyst dewetting is likely.

Our dynamic experiments revealed a fast response of the hydrogen release in the CPR. The system adapted quickly to variations in temperature and H12-BT feed and proved its capability for flexible hydrogen supply. To assess the technical relevance of the achieved dynamics, we applied reported data from a flexible CCP plant to our CPR system and found that the dynamic hydrogen demand of such a plant could be covered very well by our LOHC dehydrogenation system operating on H12-BT.

CRediT authorship contribution statement

P. Nathrath: Writing – original draft, Investigation, Formal analysis, Data curation. **T. Hein:** Writing – review & editing, Investigation, Data curation. **M. Li:** Investigation. **F. Lederle:** Writing – review & editing, Investigation. **P. Wasserscheid:** Writing – review & editing, Resources, Funding acquisition. **E.G. Hübner:** Writing – review & editing, Supervision, Resources, Project administration, Funding acquisition. **P. Schühle:** Writing – review & editing, Supervision, Resources, Project administration, Funding acquisition, Conceptualization.

Declaration of competing interest

The authors declare the following financial interests/personal relationships which may be considered as potential competing interests: Peter Wasserscheid reports a relationship with Hydrogenious LOHC Technologies GmbH that includes: board membership and consulting or advisory. If there are other authors, they declare that they have no known competing financial interests or personal relationships that could have appeared to influence the work reported in this paper.

Acknowledgements

The authors thank the German Federal Ministry for Economic Affairs and Energy for the financial support in the LOReley project (Grant number: 03EI3023A and 03EI3023F). We also like to appreciate the collaboration with Kelvion PHE GmbH (Jannis Müller-Ebhardt and Alexander Gernhardt), who supported us in the design and manufacture the reactor prototype. The authors further gratefully acknowledge the German Federal Ministry of Research, Technology and Space for funding of the BMFTR Junior Research Group FAIR-H2 (Grant number: 03SF0730). Additionally, we express our gratitude to Dr. Andreas Hutzler from Helmholtz Institute Erlangen-Nürnberg for Renewable Energy for conducting the TEM measurements.

Appendix A. Supplementary data

Supplementary data to this article can be found online at.

Data availability

Research data to this article can be found online at zenodo https://doi.org/10.5281/zenodo.14673087.

References

[1] Panwar NL, Kaushik SC, Kothari S. Role of renewable energy sources in environmental protection: a review. Renew Sustain Energy Rev 2011;15:1513–24. https://doi.org/10.1016/j.rser.2010.11.037.

[2] Kebede AA, Kalogiannis T, Van Mierlo J, Berecibar M. A comprehensive review of stationary energy storage devices for large scale renewable energy sources grid integration. Renew Sustain Energy Rev 2022;159:112213. https://doi.org/10.1016/j.rser.2022.112213.

[3] European Commission. Directorate general for economic and financial affairs. In: Busch S, Kasdorp R, Koolen D, Mercier A, Spooner M, editors. The development of renewable energy in the electricity market; 2023. https://doi.org/10.2765/411281.

[4] Sansavini G, Gabrielli P, Gjorgiev B, Akbari B, Brodnicke L, Lonergan K, Wu R, Kocher T, Berger J, Collenberg W. Changing energy mix and its impact on grid stability. 18, https://doi.org/10.3929/ETHZ-B-000529565; 2021.

[5] Ueckerdt F, Kempener R. From baseload to peak: renewables provide a reliable solution. 2015.

[6] Sinn H-W. Buffering volatility: a study on the limits of Germany's energy revolution. Eur Econ Rev 2017;99:130–50. https://doi.org/10.1016/j.euroecorev.2017.05.007.

[7] Abrell J, Rausch S, Streitberger C. Buffering volatility: storage investments and technology-specific renewable energy support. Energy Econ 2019;84:104463. https://doi.org/10.1016/j.eneco.2019.07.023.

[8] Hermann H, Gores S, Nissen C. Matching of power plants by fuel, European topic centre on climate change mitigation and energy. https://www.eionet.europa.eu/etcs/etc-cme/products/etc-cme-reports/etc-cme-report-10-2021-matching-of-power-plants-by-fuel/@@download/file/ETC_CME_Report_10-2021_final.pdf. [Accessed 28 April 2025].

[9] Gorenstein Dedecca J, Ansarin M, Bene C, van Delzen T, van Nuffel L, Jagtenberg H. Increasing flexibility in the EU energy system - technologies and policies to enable the integration of renewable electricity sources, publication for the committee on industry, research and energy, policy department for transformation, innovation and health. Luxembourg: European Parliament; 2025. https://www.europarl.europa.eu/RegData/etudes/STUD/2025/769347/ECTI_STU(2025)769347_EN.pdf. [Accessed 29 April 2025].

[10] Emdadi K, Gandomkar M, Nikoukar J. Energy scheduling of renewable integrated system with hydrogen storage in distribution grid including charging and hydrogen stations of electric vehicles. Sci Rep 2025;15:16347. https://doi.org/10.1038/s41598-025-99697-z.

[11] Risco-Bravo A, Varela C, Bartels J, Zondervan E. From green hydrogen to electricity: a review on recent advances, challenges, and opportunities on power-to-hydrogen-to-power systems. Renew Sustain Energy Rev 2024;189:113930. https://doi.org/10.1016/j.rser.2023.113930.

[12] Wu D, Wang D, Ramachandran T, Holladay J. A techno-economic assessment framework for hydrogen energy storage toward multiple energy delivery pathways and grid services. Energy 2022;249:123638. https://doi.org/10.1016/j.energy.2022.123638.

[13] Haoxin D, Qiyuan D, Chaojie L, Nian L, Zhang W, Hu M, Xu C. A comprehensive review on renewable power-to-green hydrogen-to-power systems: green hydrogen production, transportation, storage, re-electrification and safety. Appl Energy 2025;390:125821. https://doi.org/10.1016/j.apenergy.2025.125821.

[14] Kroll F, Schörner M, Schmidt M, Kohler FTU, Albert J, Schühle P. Hydrogen production from wet biomass via a formic acid route under mild conditions. Int J Hydrogen Energy 2024;62:959–68. https://doi.org/10.1016/j.ijhydene.2024.03.163.

[15] Koj JC, Zapp P, Wieland C, Görner K, Kuckshinrichs W. Green hydrogen production by PEM water electrolysis up to the year 2050: prospective life cycle assessment using learning curves. J Ind Ecol 2025;29:145–58. https://doi.org/10.1111/jiec.13592.

[16] Preuster P, Papp C, Wasserscheid P. Liquid organic hydrogen carriers (LOHCs): toward a hydrogen-free hydrogen economy. Acc Chem Res 2017;50:74–85. https://doi.org/10.1021/acs.accounts.6b00474.

[17] AlRafea K, Fowler M, Elkamel A, Hajimiragha A. Integration of renewable energy sources into combined cycle power plants through electrolysis generated hydrogen in a new designed energy hub. Int J Hydrogen Energy 2016;41:16718–28. https://doi.org/10.1016/j.ijhydene.2016.06.256.

[18] Christidis A, Wasike-Schalling A, Arriens J. H2-Ready gas-fired power plants. https://reiner-lemoine-institut.de/wp-content/uploads/2023/11/RLI-Study-H2-ready-EN.pdf; 2023.

[19] Abuzayed A, Liebensteiner M, Hartmann N. Hydrogen-ready power plants: optimizing pathways to a decarbonized energy system in Germany. Appl Energy 2025;395:126228. https://doi.org/10.1016/j.apenergy.2025.126228.

[20] Preuster P, Alekseev A, Wasserscheid P. Hydrogen storage technologies for future energy systems. Annu Rev Chem Biomol Eng 2017;8:445–71. https://doi.org/10.1146/annurev-chembioeng-060816-101334.

[21] Fikrt A, Brehmer R, Milella V-O, Müller K, Bösmann A, Preuster P, Alt N, Schlücker E, Wasserscheid P, Arlt W. Dynamic power supply by hydrogen bound to a liquid organic hydrogen carrier. Appl Energy 2017;194:1–8. https://doi.org/10.1016/j.apenergy.2017.02.070.

[22] Teichmann D, Arlt W, Schlücker E, Wasserscheid P. Transport and storage of hydrogen via liquid organic hydrogen carrier (LOHC) systems. In: Stolten ProfDrD, Emonts DrB, editors. Hydrogen science and engineering : materials, processes, systems and technology. first ed. Wiley; 2016. p. 811–30. https://doi.org/10.1002/9783527674268.ch33.

[23] Jorschick H, Geißelbrecht M, Eßl M, Preuster P, Bösmann A, Wasserscheid P. Benzyltoluene/dibenzyltoluene-based mixtures as suitable liquid organic hydrogen carrier systems for low temperature applications. Int J Hydrogen Energy 2020;45:14897–906. https://doi.org/10.1016/j.ijhydene.2020.03.210.

[24] Brückner N, Obesser K, Bösmann A, Teichmann D, Arlt W, Dungs J, Wasserscheid P. Evaluation of industrially applied heat-transfer fluids as liquid organic hydrogen carrier systems. ChemSusChem 2014;7:229–35. https://doi.org/10.1002/cssc.201300426.

[25] Gianotti E, Taillades-Jacquin M, Rozière J, Jones DJ. High-purity hydrogen generation via dehydrogenation of organic carriers: a review on the catalytic process. ACS Catal 2018;8:4660–80. https://doi.org/10.1021/acscatal.7b04278.

[26] Gemechu DN, Mohammed AM, Redi M, Bessarabov D, Mekonnen YS, Obodo KO. First principles-based approaches for catalytic activity on the dehydrogenation of liquid organic hydrogen carriers: a review. Int J Hydrogen Energy 2023;48:33186–206. https://doi.org/10.1016/j.ijhydene.2023.05.072.

[27] Ellert A, Herold F, Rønning M, Hutzler A, Piccirilli L, Janssens TVW, Vennestrøm PNR, Wasserscheid P, Schühle P. Phosphorus-modification of Pt/Al2O3 catalysts improves dispersion and cycloalkane dehydrogenation activity. J Catal 2024;436:115607. https://doi.org/10.1016/j.jcat.2024.115607.

[28] Müller K, Stark K, Emel'yanenko VN, Varfolomeev MA, Zaitsau DH, Shoifet E, Schick C, Verevkin SP, Arlt W. Liquid organic hydrogen carriers: thermophysical and thermochemical studies of Benzyl- and dibenzyl-toluene derivatives. Ind Eng Chem Res 2015;54:7967–76. https://doi.org/10.1021/acs.iecr.5b01840.

[29] Rüde T, Dürr S, Preuster P, Wolf M, Wasserscheid P. Benzyltoluene/perhydro benzyltoluene – pushing the performance limits of pure hydrocarbon liquid organic hydrogen carrier (LOHC) systems. Sustain Energy Fuels 2022;6:1541–53. https://doi.org/10.1039/D1SE01767E.

[30] Auer F, Blaumeiser D, Bauer T, Bösmann A, Szesni N, Libuda J, Wasserscheid P. Boosting the activity of hydrogen release from liquid organic hydrogen carrier systems by sulfuradditives to Pt on alumina catalysts. Catal Sci Technol 2019:3537–47. https://doi.org/10.1039/c9cy00817a.

[31] Okada Y, Shimura M, Okada Yoshimi, Shimura Mitsunori. "Development of large-scale H2 storage and transportation technology with liquid organic hydrogen carrier (LOHC). In: Proceedings of the 21st joint GCC-Japan environment symposium. Quatar: Doha; 2013. https://www.jccp.or.jp/international/conference/docs/15rev-chiyoda-mr-shimura-chiyoda-h2-sturage-and-transpor.pdf. [Accessed 17 October 2024].

[32] Willer M, Preuster P, Geißelbrecht M, Wasserscheid P. Continuous dehydrogenation of perhydro benzyltoluene and perhydro dibenzyltoluene in a packed bed vertical tubular reactor – the role of LOHC evaporation. Int J Hydrogen Energy 2024;57:1513–23. https://doi.org/10.1016/j.ijhydene.2024.01.031.

[33] Kadar J, Gackstatter F, Ortner F, Wagner L, Willer M, Preuster P, Wasserscheid P, Geißelbrecht M. Boosting power density of hydrogen release from LOHC systems by an inverted fixed-bed reactor design. Int J Hydrogen Energy 2024;59:1376–87. https://doi.org/10.1016/j.ijhydene.2024.02.096.

[34] Ye H-L, Liu S-X, Zhang C, Cai Y-Q, Shi Y-F. Dehydrogenation of methylcyclohexane over Pt-based catalysts supported on functional granular activated carbon. RSC Adv 2021;11:29287–97. https://doi.org/10.1039/D1RA05480E.

[35] Willer M, Preuster P, Malgaretti P, Harting J, Wasserscheid P. Heat transfer to a catalytic multiphase dehydrogenation reactor. Int J Hydrogen Energy 2024;80:1011–20. https://doi.org/10.1016/j.ijhydene.2024.07.073.

[36] Solymosi T, Auer F, Dürr S, Preuster P, Wasserscheid P. Catalytically activated stainless steel plates for the dehydrogenation of perhydro dibenzyltoluene. Int J Hydrogen Energy 2021;46:34797–806. https://doi.org/10.1016/j.ijhydene.2021.08.040.

[37] Tschudin S, Shido T, Prins R, Wokaun A. Characterisation of catalysts used in wall reactors for the catalytic dehydrogenation of methylcyclohexane. J Catal 1999;181:113–23. https://doi.org/10.1006/jcat.1998.2283.

[38] Théron F. Characterization of the performances of an innovative heat-exchanger/reactor. Chem Eng Process 2014:12. https://doi.org/10.1016/j.cep.2014.04.005.

[39] Muley A, Manglik RM. Experimental study of turbulent flow heat transfer and pressure drop in a plate heat exchanger with chevron plates. J Heat Tran 1999;121:110–7. https://doi.org/10.1115/1.2825923.

[40] Anxionnaz Z, Cabassud M, Gourdon C, Tochon P. Heat exchanger/reactors (HEX reactors): concepts, technologies: state-of-the-art. Chem Eng Process 2008:22. https://doi.org/10.1016/j.cep.2008.06.012.

[41] Jo Y, Oh J, Kim D, Park JH, Baik JH, Suh Y-W. Recent progress in dehydrogenation catalysts for heterocyclic and homocyclic liquid organic hydrogen carriers. Kor J Chem Eng 2022;39:20–37. https://doi.org/10.1007/s11814-021-0947-5.

[42] Meille V. Review on methods to deposit catalysts on structured surfaces. Appl Catal Gen 2006;315:1–17. https://doi.org/10.1016/j.apcata.2006.08.031.

[43] Bera S, Udayabhanu G, Narayan R, Rout TK. Methodologies of application of Sol-Gel based solution onto substrate: a review. J Coat Sci Technol 2016;3:9–22. https://doi.org/10.6000/2369-3355.2016.03.01.2.

[44] Montebelli A, Visconti CG, Groppi G, Tronconi E, Cristiani C, Ferreira C, Kohler S. Methods for the catalytic activation of metallic structured substrates. Catal Sci Technol 2014;4:2846–70. https://doi.org/10.1039/C4CY00179F.

[45] Barrow DA, Petroff TE, Sayer M. Thick ceramic coatings using a sol gel based ceramic-ceramic 0–3 composite. Surf Coating Technol 1995;76–77:113–8. https://doi.org/10.1016/0257-8972(95)02562-6.

[46] Nathrath P, Raed Ramzi Y, Bierling M, Thiele S, Wasserscheid P, Schühle P. Highly durable spray-coated plate catalyst for the dehydrogenation of perhydro benzyltoluene. Catal Sci Technol 2024;14:980–9. https://doi.org/10.1039/D3CY01158E.

[47] Sun H, Li J, Liu M, Yang D, Li F. A review of effects of femtosecond laser parameters on metal surface properties. Coatings 2022;12:1596. https://doi.org/10.3390/coatings12101596.

[48] Vorobyev AY, Guo C. Direct femtosecond laser surface nano/microstructuring and its applications. Laser Photon Rev 2013;7:385–407. https://doi.org/10.1002/lpor.201200017.

[49] Ahmmed K, Grambow C, Kietzig A-M. Fabrication of micro/nano structures on metals by femtosecond laser micromachining. Micromachines 2014;5:1219–53. https://doi.org/10.3390/mi5041219.

[50] Li X, Yuan C, Yang H, Li J, Huang W, Tang D, Xu Q. Morphology and composition on Al surface irradiated by femtosecond laser pulses. Appl Surf Sci 2010;256:4344–9. https://doi.org/10.1016/j.apsusc.2010.02.029.
[51] Balchev I, Minkovski N, Marinova Ts, Shipochka M, Sabotinov N. Composition and structure characterization of aluminum after laser ablation. Mater Sci Eng, B 2006;135:108–12. https://doi.org/10.1016/j.mseb.2006.08.042.
[52] Xu S, Tan L, Yao C, Miao X, Lü H, Jiang X, Yuan X. Anti-reflective and wetting properties of femtosecond pulsed laser textured Al alloy surfaces. Optik 2021;242:167293. https://doi.org/10.1016/j.ijleo.2021.167293.
[53] Lange K, Hördemann C, Schulz-Ruhtenberg M, Caro J. Porous nickel nano-foam by femtosecond laser structuring for supercapacitor application. Chemelectrochem 2018;5:3688–94. https://doi.org/10.1002/celc.201801152.
[54] Nathrath P, Baier B, Herz N, Wituschek S, Ramzi YR, Merklein M, Li M, Lederle F, Wasserscheid P, Hübner EG, Schühle P. Hydrogen release from liquid organic hydrogen carrier using plate catalysts in continuous and dynamic operation. Chem Eng J 2025;506:159878. https://doi.org/10.1016/j.cej.2025.159878.
[55] Wöbbeking K, Li M, Hübner EG, Schade W. Conical microstructuring of titanium by reactive gas assisted laser texturing. RSC Adv 2019;9:37598–607. https://doi.org/10.1039/C9RA05918K.
[56] Wöbbeking K, Li M, Schade W, Hübner EG. Microconical surface structuring of aluminium tubes by femtosecond laser processing. J Phys Commun 2020;4:111001. https://doi.org/10.1088/2399-6528/abc6b2.
[57] Fedorov R, Lederle F, Li M, Olszok V, Wöbbeking K, Schade W, Hübner EG. Formation of titanium nitride, titanium carbide, and silicon carbide surfaces by high power femtosecond laser treatment. ChemPlusChem 2021;86:1231–42. https://doi.org/10.1002/cplu.202100118.
[58] Bergeret G, Gallezot P. Particle size and dispersion measurements. In: Ertl G, Knözinger H, Schüth F, Weitkamp J, editors. Handbook of heterogeneous catalysis. first ed. Wiley; 2008. p. 738–65. https://doi.org/10.1002/9783527610044.hetcat0038.
[59] Geißelbrecht M. Prozessintensivierung für die Wasserstofffreisetzung aus flüssigen organischen Wasserstoffträgern. Dissertation: Friedrich-Alexander-Universität Erlangen-Nürnberg (FAU); 2021.
[60] Fraunhofer-Institut für Solare Energiesysteme ISE. Energy-Charts 2023. https://www.energy-charts.info. [Accessed 19 July 2023].
[61] Datsevich LB. Oscillation theory. Appl Catal Gen 2005;294:22–33. https://doi.org/10.1016/j.apcata.2005.06.024.
[62] Solymosi T, Geißelbrecht M, Mayer S, Auer M, Leicht P, Terlinden M, Malgaretti P, Bösmann A, Preuster P, Harting J, Thommes M, Vogel N, Wasserscheid P. Nucleation as a rate-determining step in catalytic gas generation reactions from liquid phase systems. Sci Adv 2022;8. https://doi.org/10.1126/sciadv.ade3262.ade3262.
[63] Taylor S, Fabbri E, Levecque P, Schmidt TJ, Conrad O. The effect of platinum loading and surface morphology on oxygen reduction activity. Electrocatalysis 2016;7:287–96. https://doi.org/10.1007/s12678-016-0304-3.
[64] Duarte HA, Sad ME, Apesteguía CR. Aqueous phase reforming of sorbitol on Pt/Al2O3: effect of metal loading and reaction conditions on H2 productivity. Int J Hydrogen Energy 2016;41:17290–6. https://doi.org/10.1016/j.ijhydene.2016.07.071.
[65] Auer F, Hupfer A, Bösmann A, Szesni N, Wasserscheid P. Influence of the nanoparticle size on hydrogen release and side product formation in liquid organic hydrogen carrier systems with supported platinum catalysts. Catal Sci Technol 2020;10:6669–78. https://doi.org/10.1039/D0CY01173H.
[66] Modisha P, Bessarabov D. Stress tolerance assessment of dibenzyltoluene-based liquid organic hydrogen carriers. Sustain Energy Fuels 2020;4:4662–70. https://doi.org/10.1039/D0SE00625D.
[67] Bong B, Mebrahtu C, Jurado D, Bösmann A, Wasserscheid P, Palkovits R. Hydrogen loading and release potential of the LOHC system benzyltoluene/perhydro benzyltoluene over S–Pt/TiO $_2$ catalyst. ACS Eng Au 2024;4:359–67. https://doi.org/10.1021/acsengineeringau.4c00003.
[68] Ellert A, Schmacks M, Braun MJ, Piccirilli L, Janssens TVW, Wasserscheid P, Schühle P. Continuous dehydrogenation of perhydro benzyltoluene in a catalytic finned tube reactor. Ind Eng Chem Res 2025. https://doi.org/10.1021/acs.iecr.4c04254.
[69] Heublein N, Stelzner M, Sattelmayer T. Hydrogen storage using liquid organic carriers: equilibrium simulation and dehydrogenation reactor design. Int J Hydrogen Energy 2020;45:24902–16. https://doi.org/10.1016/j.ijhydene.2020.04.274.
[70] Rüde T, Lu Y, Anschütz L, Blasius M, Wolf M, Preuster P, Wasserscheid P, Geißelbrecht M. Performance of continuous hydrogen production from perhydro benzyltoluene by catalytic distillation and heat integration concepts with a fuel cell. Energy Tech 2023;11:2201366. https://doi.org/10.1002/ente.202201366.
[71] Henseler J, Schärfe T, Steffen J, Görling A, Geißelbrecht M, Wasserscheid P. Detailed analysis of coke precursor formation in catalytic perhydro benzyltoluene dehydrogenation processes. Fuel 2025;398:135500. https://doi.org/10.1016/j.fuel.2025.135500.